Advances in Military Technology
Vol. 19, No. 1, 2024, pp. 165-175
ISSN 1802-2308, eISSN 2533-4123
DOI 10.3849/aimt.01878

Dynamics of Heavy Mechanized Bridge During Span-Lowering Process

Tran Duc Thang[1], Le Van Duong[1], Chu Van Dat[1], Cu Xuan Phong[1*], and Bui Van Hai[2]

[1] *Le Quy Don Technical University, Viet Nam*
[2] *Hanoi University of Industry, Viet Nam*

The manuscript was received on 7 January 2024 and was accepted after revision for publication as research paper on 25 May 2024.

Abstract:

Heavy mechanized bridge is utilized to be rapidly deployed as a temporary bridge to facilitate the movement of vehicles and personnel across obstacles. This paper presents a dynamic model of the TMM-3M heavy mechanized bridge during the span-lowering process, including considerations of cable deformation, rear outriggers, elasticity of tire, and front suspension system. Based on the dynamic model, the authors establish a system of differential equations describing the oscillation of the system using Lagrangian equations of the second kind. The article provides a fundamental basis for studying the entire process of deploying the TMM-3M bridge and aims to improve the rear outriggers and cable winding system to reduce bridge deployment time.

Keywords:

heavy mechanized bridge, elastic cable, military bridge

1 Introduction

Heavy mechanized bridge, in general, is specialized machinery that can be used for both military and civilian purposes to rapidly deploy a temporary bridge, facilitating the quick establishment of a mobile route for vehicles and pedestrians to overcome obstacles such as shallow gaps, rivers, and streams, or to support rescue and relief efforts by creating passageways over challenging terrain. Heavy mechanized bridges are specially manufactured and utilized in countries such as the United States, India, Germany, Russia, the Czech Republic, and China [1, 2]. The TMM-3M bridge (Fig. 1) is a heavy mechanized bridge produced by Russia. “TMM” is an abbreviation for the Russian phrase “Тяжелый механизированный мост” – heavy mechanized bridge, while “3M” refers to the version of the TMM bridge manufactured in the 1970s-1980s.

[*] *Corresponding author: Le Quy Don Technical University, 236 Hoang Quoc Viet, Ha Noi, Viet Nam. Phone: +84 986 70 43 93, E-mail: phong.cx@lqdtu.edu.vn*

The chassis of this equipment can be either wheeled or tracked. For wheeled chassis–based heavy mechanized bridges deployed in an upright configuration, the deployment process consists of four main stages in the following order: the frame lifting stage, the span opening stage, the lowering stage, and the intermediate bridge support lowering stage. When deploying a single-span bridge, there are only the first three stages. The deployment process of wheeled chassis–based heavy mechanized bridges depends on the geological conditions at the deployment site, allowing the equipment to be deployed only when ensuring the soil stiffness and the horizontal and vertical slopes of the terrain.

Research on heavy mechanized bridges up to the present moment remains highly limited in publication. This is partly due to the inherently secretive nature of military operations in various countries and the limited dissemination of usage beyond practical applications [3-5]. Most publications primarily take the form of overviews regarding the development of military bridges by various countries. There is a lack of publications on the dynamics of the operational processes of this equipment. Considering the working characteristics of wheeled chassis–based heavy mechanized bridges during the bridge–laying phase, we can observe similarities with the operation of wheeled cranes in the process of lifting and lowering loads [6-11]. Research on the dynamics of wheeled or tracked cranes has garnered significant attention from scientists, with numerous studies dedicated to understanding their mechanical aspects. In [6-8, 11, 12], the authors investigated the dynamics of wheeled or tracked cranes during their operational processes, including the deformation of cables during lifting and lowering tasks.

Fig. 1 Heavy mechanized bridge TMM–3M

However, the dynamic analysis of the operational processes of a specialized system, such as the lifting framework – bridge span – intermediate support bridge on heavy mechanized bridges has not been clearly published or documented. In this article, the authors conducted a dynamic analysis of the heavy mechanized bridge TMM–3M during the span-lowering process. The research results serve as a basis for designing a control strategy for the bridge deployment process and improving the rear outriggers of the equipment.

2 Dynamic Model of Heavy Mechanized Bridge During the Span–Lowering Process

2.1 System Description

The span-lowering process during the deployment of a heavy mechanized bridge occurs with no movement of the base vehicle. During the span-lowering phase, it is assumed that the TMM–3M heavy mechanized bridge is on a flat and perfectly rigid surface. The two rear outriggers are lowered to the ground to eliminate lateral and longitudinal inclinations. At this point, the rear bridge of the base vehicle is considered to have no impact on the oscillation of the vehicle. The lifting frame is linked with the vehicle chassis through hinge joints and is pushed by two cylinders while being pulled by two linkages. In this process, the lifting frame is considered rigidly connected to the vehicle chassis, suitable for practical working conditions. The masses are considered as perfectly rigid and placed at the center of each part, including the non-suspended front bridge mass m_1, the suspended mass on the base vehicle m_2, the lifting frame mass m_3, and the mass of the bridge span – intermediate bridge support m_s. The model describes the dynamics of the TMM–3M heavy mechanized bridge deployment during the span-lowering process as a 2D model (Fig. 2).

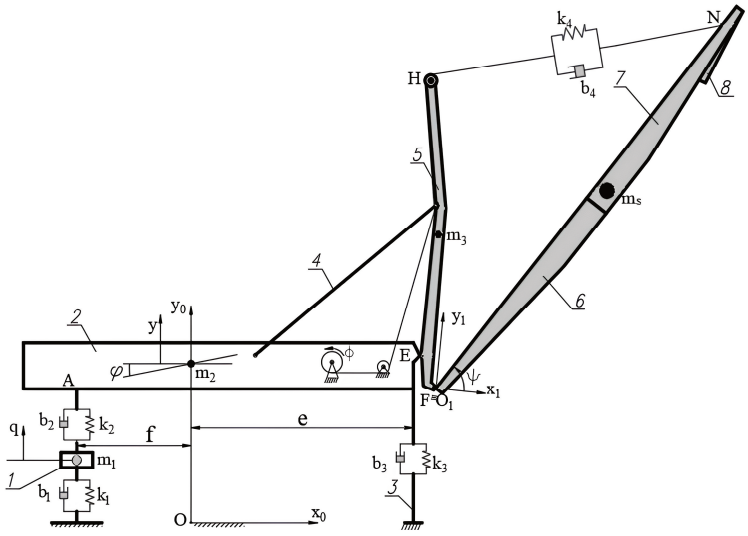

Fig. 2 Dynamics of heavy mechanized bridge during span-lowering process
1 – front axle; 2 – chassis; 3 – rear outriggers; 4 – linkages; 5 – lifting frame;
6 – front half–span of the bridge; 7 – rear half–span of the bridge;
8 – intermediate bridge support

The entire mechanical system is positioned within the fixed coordinate system Ox_0y_0. The vehicle body performs simultaneous translational motion along the vertical axis and rotation about an axis passing through the center of mass, perpendicular to the symmetric vertical plane of the chassis. The bridge span undergoes rotational motion around the hinge joint F, connecting the span and the lifting frame. The vehicle body is considered to oscillate along the vertical axis. The cable drum receives torque from

the engine through the power transmission system to drive the process of lowering the bridge span.

Besides the remaining geometric dimensions described in Fig. 2, several other symbols are conventionally defined as follows:

b_1 and k_1 – represent the damping coefficient and stiffness coefficient of the front tires, respectively;

b_2 and k_2 – the damping coefficient and stiffness coefficient of the front suspension system, respectively;

b_3 and k_3 – represent the damping coefficient and stiffness coefficient of the rear outriggers, respectively;

b_4 and k_4 – represent the damping coefficient and stiffness coefficient of the main cable, respectively;

G_1, G_2, G_3 and G_s – correspondingly represent the center of mass positions of masses m_1, m_2, m_3, m_s in a system;

J_2, J_3, J_s and J_t – respectively represent the moments of inertia of the body vehicle, the lifting frame, the bridge span and the cable winding drum, respectively;

H_1 and H_2 – respectively represent the initial heights of the center of mass of masses m_1 and m_2, respectively.

Some geometric factors are symbolized as follows:

$$l_1 = G_2F; \quad l_2 = G_2G_3; \quad l_3 = G_2H; \quad l_4 = NF; \quad l_5 = FG_s; \quad l_6 = FH$$

$$\alpha_1 = \angle FG_2L; \quad \alpha_2 = \angle G_3G_2L; \quad \alpha_3 = \angle HG_2L; \quad \alpha_5 = \angle NFG_s; \quad \alpha_6 = \angle HFG_2$$

in which G_2L always has a vertical direction along the chassis.

2.2 System Description

Generalized coordinates have been assumed whose vector (Fig. 2) has the form:

$$\begin{bmatrix} q & y & \varphi & \phi & \psi \end{bmatrix}^{\mathrm{T}}$$

where

q [m] – vertical displacement of the unsprung mass of the front axle;
y [m] – vertical displacement of the center of mass of the chassis;
φ [rad] – pitch angle of the chassis;
ϕ [rad] – angle of rotation of the cable winding drum;
ψ [rad] – angular displacement of the bridge span.

The kinetic energy of the system:

The kinetic energy of the system includes the kinetic energy of the unsprung mass of the front axle, the kinetic energy of the suspended mass on the chassis, the kinetic energy of the lifting frame, the kinetic energy of the bridge span, and the kinetic energy of the cable winding drum, and is determined by the expression:

$$\begin{aligned} T = {} & \frac{1}{2}m_1\dot{q}^2 + \frac{1}{2}m_2\dot{y}^2 + \frac{1}{2}\left(J_2 + J_3\right)\dot{\varphi}^2 + \frac{1}{2}m_3\left\{\begin{matrix} l_2^{\,2}\dot{\varphi}^2 + \dot{y}^2 + \\ +2l_2\cos\left(\varphi + \alpha_2\right)\dot{\varphi}\dot{y} \end{matrix}\right\} \\ & + \frac{1}{2}m_s\left\{\begin{matrix} l_1^{\,2}\dot{\varphi}^2 + \dot{y}^2 + l_5^{\,2}\left(\dot{\varphi}+\dot{\psi}\right)^2 + 2l_1l_5\cos\left(\psi - \alpha_5\right)\left(\dot{\varphi}+\dot{\psi}\right)\dot{\varphi} + \\ +2l_1\cos\left(\varphi - \alpha_1\right)\dot{\varphi}\dot{y} + 2l_5\cos\left(\varphi + \psi - \alpha_1 - \alpha_5\right)\left(\dot{\varphi}+\dot{\psi}\right)\dot{y} \end{matrix}\right\} \\ & + \frac{1}{2}J_s\dot{\psi}^2 + \frac{1}{2}J_t\dot{\phi}^2 \end{aligned} \tag{1}$$

The potential energy of the system:

The potential energy of the system includes gravitational potential energy and elastic potential energy. Firstly, we have the cable elongation during the lowering process, which includes static deformation and dynamic deformation determined by the expressions [6]:

$$\Delta l = \Delta l_{\mathrm{s}} + \Delta l_{\mathrm{d}} \tag{2}$$

The static cable tension force F_{cs} at any given time is determined through the equation of moment equilibrium with respect to the axis passing through point F, expressed as:

$$\sum M\left(K\right) = F_{\mathrm{cs}} r_{\mathrm{c}} - m_{\mathrm{s}} g l_5 \cos\left(\varphi + \psi - \alpha_1 - \alpha_5\right) = 0 \tag{3}$$

in which r_{c} is the distance from F to the line of action of the force vector $\vec{F}_{\mathrm{cs}}$, and is determined by the expression:

$$r_{\mathrm{c}} = \frac{l_6 l_4 \sin\left(\psi + \alpha_6\right)}{\sqrt{l_1^{\,2} + l_3^{\,2} + l_4^{\,2} - 2l_1 l_3 \cos\left(\alpha_3 + \alpha_1\right) + 2l_1 l_4 \cos\psi - 2l_3 l_4 \cos\left(\psi - \alpha_3 - \alpha_1\right)}} \tag{4}$$

The static deformation is determined by the maximum static cable tension force $F_{\mathrm{cs\,max}}$ occurring in the cable at the end of the span–lowering process, and is given by:

$$\Delta l_{\mathrm{s}} = \frac{F_{\mathrm{csmax}}}{k_4} \tag{5}$$

The dynamic deformation of the cable during the span–lowering process is determined as follows:

$$\Delta l_{\mathrm{d}} = S - S_0 - R_{\mathrm{t}}\left(\phi - \phi_0\right) \tag{6}$$

In the expression (6), S is the length of the cable segment from H to N at any given time, S_0 is the initial length of the cable segment from H to N; $\mathrm{R_t}$ is the radius of the cable winding drum; ϕ_0 and ψ_0 are the respective angles of rotation of the cable winding drum and the angle determining the position of the bridge span at the initial time. These quantities are determined by the following expressions:

$$S = \sqrt{l_1^{\,2} + l_2^{\,2} + l_4^{\,2} - 2l_1 l_2 \cos\left(\alpha_2 + \alpha_1\right) + 2l_1 l_4 \cos\psi - 2l_2 l_4 \cos\left(\psi - \alpha_2 - \alpha_1\right)} \tag{7}$$

$$S_0 = \sqrt{l_1^{\,2} + l_2^{\,2} + l_4^{\,2} - 2l_1 l_2 \cos\left(\alpha_2 + \alpha_1\right) + 2l_1 l_4 \cos\psi_0 - 2l_2 l_4 \cos\left(\psi_0 - \alpha_2 - \alpha_1\right)} \tag{8}$$

We have the expression defining the total potential energy of the system as:

$$\Pi = \left\{ \begin{array}{l} m_1 g\left(q + H_1\right) + m_2 g\left(y + H_2\right) + m_3 g\left[y + H_2 + l_2 \sin\left(\varphi + \alpha_2\right)\right] + \\ + m_{\mathrm{s}} g\left[y + H_2 + l_1 \sin\left(\varphi - \alpha_1\right) + l_5 \sin\left(\varphi + \psi - \alpha_1 - \alpha_5\right)\right] + \\ + \frac{1}{2} k_4 \Delta l^2 + \frac{1}{2} k_2 \left(y - q - f\varphi\right)^2 + \frac{1}{2} k_1 q^2 + \frac{1}{2} k_3 \left(y + e\varphi\right)^2 \end{array} \right\} \tag{9}$$

The total dissipative energy of the system

The total dissipative energy of the system is determined by the following expression:

$$\phi = \frac{1}{2} b_2 \left(\dot{y} - \dot{q} - f\dot{\varphi}\right)^2 + \frac{1}{2} b_1 \dot{q}^2 + \frac{1}{2} b_3 \left(\dot{y} + e\dot{\varphi}\right)^2 + \frac{1}{2} b_4 \left(\dot{\Delta l}\right)^2 \tag{10}$$

In the expression (10), $\Delta\dot{l}$ is determined as follows:

$$\Delta\dot{l} = \frac{\left[-l_1 l_4 \sin\psi + l_2 l_4 \sin\left(\psi - \alpha_2 - \alpha_1\right)\right]\dot{\psi}}{\sqrt{\begin{array}{l} l_1^{\,2} + l_2^{\,2} + l_4^{\,2} - 2l_1 l_2 \cos\left(\alpha_2 + \alpha_1\right) + \\ + 2l_1 l_4 \cos\psi - 2l_2 l_4 \cos\left(\psi - \alpha_2 - \alpha_1\right) \end{array}}} + R_t\dot{\phi} \tag{11}$$

Generalized Forces

The static moment M_t at any given time due to the static cable tension force acting on the cable winding drum is:

$$M_t = \frac{m_s g R_t l_5 \cos\left(\varphi + \psi - \alpha_1 - \alpha_5\right)\sqrt{\begin{array}{l} l_1^{\,2} + l_3^{\,2} + l_4^{\,2} - 2l_1 l_3 \cos\left(\alpha_3 + \alpha_1\right) + \\ + 2l_1 l_4 \cos\psi - 2l_3 l_4 \cos\left(\psi - \alpha_3 - \alpha_1\right) \end{array}}}{l_6 l_4 \sin\left(\psi + \alpha_6\right)} \tag{12}$$

From the expression (12), we can determine the maximum static moment $M_{t\,max}$ due to the load acting on the cable winding drum at the end of the span–lowering process when φ_{min}, ψ_{min}.

The brake moment M_p is taken with a safety factor of 1.25. The brake moment ensures that the bridge span can be stopped at any time without falling, ensuring safety. In this case, the necessary value of the brake moment to be applied to the cable winding drum is [11]:

$$M_p = 1.25 M_{t\,max} \tag{13}$$

To drive the cable winding drum, a torque M_e is required from the engine to the cable winding drum. M_e must overcome the resistance of the brake moment after subtracting the torque due to the load pulling the cable winding drum during lowering. Therefore, the total external torque acting on the cable winding drum to rotate it is determined by the expression:

$$M = M_e - M_p + M_t \tag{14}$$

The virtual work done by external forces acting on the system is:

$$\delta W = M\,\delta\phi \tag{15}$$

Apply the Lagrange's second kind equation to formulate the system of differential equations describing the oscillations of the system in the form:

$$\frac{\mathrm{d}}{\mathrm{d}t}\left(\frac{T}{\partial\dot{q}_i}\right) - \frac{\partial T}{\partial q_i} + \frac{\partial\Pi}{\partial q_i} + \frac{\partial\Phi}{\partial\dot{q}_i} = Q_i \quad i = 1,\cdots,5 \tag{16}$$

Substituting the expressions for kinetic energy, potential energy, and dissipative functions into Eq. (16), we obtain the system of differential equations describing the oscillations of the system as follows:

$$m_1\ddot{q} + \left(b_1 + b_2\right)\dot{q} - b_1\dot{y} + b_1 f\dot{\varphi} + \left(k_1 + k_2\right)q - k_2 y + k_2 f\varphi + m_1 g = 0 \tag{17}$$

$$\begin{aligned}&\left(m_2+m_3+m_s\right)\ddot{y}+m_s l_5\cos\left(\varphi+\psi-\alpha_1-\alpha_5\right)\ddot{\psi}+\\&+\left\{m_3 l_2\cos\left(\varphi+\alpha_2\right)+m_s\left[l_1\cos\left(\varphi-\alpha_1\right)+l_5\cos\left(\varphi+\psi-\alpha_1-\alpha_5\right)\right]\right\}\ddot{\varphi}+\\&-b_2\dot{q}+\left(b_2+b_3\right)\dot{y}+\left(b_3 e-b_2 f\right)\dot{\varphi}+\\&-\left\{m_3 l_2\sin\left(\varphi+\alpha_2\right)+m_s\left[l_1\sin\left(\varphi-\alpha_1\right)+l_5\sin\left(\varphi+\psi-\alpha_1-\alpha_5\right)\right]\right\}\dot{\varphi}^2+\\&-m_s l_5\sin\left(\varphi+\psi-\alpha_1-\alpha_5\right)\left(2\dot{\varphi}+\dot{\psi}\right)\dot{\psi}-k_2 q+\left(k_2+k_3\right)y+\\&+\left(k_3 e-k_2 f\right)\varphi+m_2 g+m_3 g+m_s g=0\end{aligned}\tag{18}$$

$$\begin{aligned}&\left\{m_3 l_2\cos\left(\varphi+\alpha_2\right)+m_s\left[l_1\cos\left(\varphi-\alpha_1\right)+l_5\cos\left(\varphi+\psi-\alpha_1-\alpha_5\right)\right]\right\}\ddot{y}+\\&+\left\{J_2+J_3+m_3 l_2^{\,2}+m_s\left[l_1^{\,2}+l_5^{\,2}+2l_1 l_5\cos\left(\psi-\alpha_5\right)\right]\right\}\ddot{\varphi}+\\&+m_s\left[l_5^{\,2}+l_1 l_5\cos\left(\psi-\alpha_5\right)\right]\ddot{\psi}+\left(b_3 e-b_2 f\right)\dot{y}+b_2 f\dot{q}+\left(b_2 f^2+b_3 e^2\right)\dot{\varphi}+\\&-m_s l_1 l_5\sin\left(\psi-\alpha_5\right)\left(2\dot{\varphi}+\dot{\psi}\right)\dot{\psi}+k_2 fq+\left(k_3 e-k_2 f\right)y+\left(k_2 f^2+k_3 e^2\right)\varphi+\\&+m_3 g l_2\cos\left(\varphi+\alpha_2\right)+m_s g\left[l_1\cos\left(\varphi-\alpha_1\right)+l_5\cos\left(\varphi+\psi-\alpha_1-\alpha_5\right)\right]=0\end{aligned}\tag{19}$$

$$J_t\ddot{\phi}-k_4 R_t\Delta l-b_4 R_t\dot{\Delta}l=M\tag{20}$$

$$\begin{aligned}&m_s l_5\cos\left(\varphi+\psi-\alpha_1-\alpha_5\right)\ddot{y}+m_s\left[l_5^{\,2}+l_1 l_5\cos\left(\psi-\alpha_5\right)\right]\ddot{\varphi}+\\&+\left(J_s+m_s l_5^{\,2}\right)\ddot{\psi}+m_s l_1 l_5\sin\left(\psi-\alpha_5\right)\dot{\varphi}^2+m_s g l_5\cos\left(\varphi+\psi-\alpha_1-\alpha_5\right)+\\&+k_4\Delta l\left(\Delta l\right)'_{\psi}+b_4\Delta\dot{l}\left(\Delta\dot{l}\right)'_{\dot{\psi}}=0\end{aligned}\tag{21}$$

In expressions (20) and (21), we have:

$$\left(\Delta l\right)'_{\psi}=\left(\Delta\dot{l}\right)'_{\dot{\psi}}=\frac{-l_1 l_4\sin\psi+l_3 l_4\sin\left(\psi-\alpha_3-\alpha_1\right)}{\sqrt{\begin{aligned}&l_1^{\,2}+l_3^{\,2}+l_4^{\,2}-2l_1 l_3\cos\left(\alpha_3+\alpha_1\right)+\\&+2l_1 l_4\cos\psi-2l_3 l_4\cos\left(\psi-\alpha_3-\alpha_1\right)\end{aligned}}}\tag{22}$$

$$\Delta\dot{l}=\frac{\left[-l_1 l_4\sin\psi+l_3 l_4\sin\left(\psi-\alpha_3-\alpha_1\right)\right]\dot{\psi}}{\sqrt{\begin{aligned}&l_1^{\,2}+l_3^{\,2}+l_4^{\,2}-2l_1 l_3\cos\left(\alpha_3+\alpha_1\right)+\\&+2l_1 l_4\cos\psi-2l_3 l_4\cos\left(\psi-\alpha_3-\alpha_1\right)\end{aligned}}}-R_t\dot{\phi}\tag{23}$$

The system of differential Eqs (17-21) is solved using numerical methods based on the application of Matlab simulation software using the Runge–Kutta algorithm. The results are presented in the following section.

3 Results and Discussion

The input parameter set for solving the system of differential equations describing the oscillations of the system includes:

$f = 2.24$ m; $e = 5.62$ m; $b_1 = 500$ Ns/m; $b_2 = 24\,000$ Ns/m; $b_3 = 500$ Ns/m; $b_4 = 100$ Ns/m; $k_1 = 800\,000$ N/m; $k_2 = 295\,000$ N/m; $k_3 = 10^7$ N/m; $k_4 = 2\times10^6$ N/m; $l_1 = 5.85$ m; $l_2 = 6.36$ m; $l_3 = 8.42$ m; $l_4 = 9.5$ m; $l_5 = 5.25$ m; $l_6 = 6.8$ m; $R_t = 0.1$ m; $\alpha_1 = 5.4^o$; $\alpha_2 = 25.6^o$; $\alpha_3 = 47.4^o$; $\alpha_5 = 3^o$; $\alpha_6 = 83^o$; $m_1 = 910$ kg; $m_2 = 8\,390$ kg; $m_3 = 1\,050$ kg; $m_s = 6\,800$ kg; $J_t = 8\,085$ kg m^2; $J_2 = 99\,252$ kg m^2; $J_3 = 8\,900$ kg m^2; $J_s = 62\,425$ kg m^2; $M_e = 5\,200$ N m.

Initial conditions: $[q_0 \quad y_0 \quad \varphi_0 \quad \phi_0 \quad \psi_0]^T = [0 \quad 0 \quad 0 \quad 0 \quad 1.6]^T$ and initial velocities of all links are all set to zero.

The survey results are depicted in Figs 3-7 below,

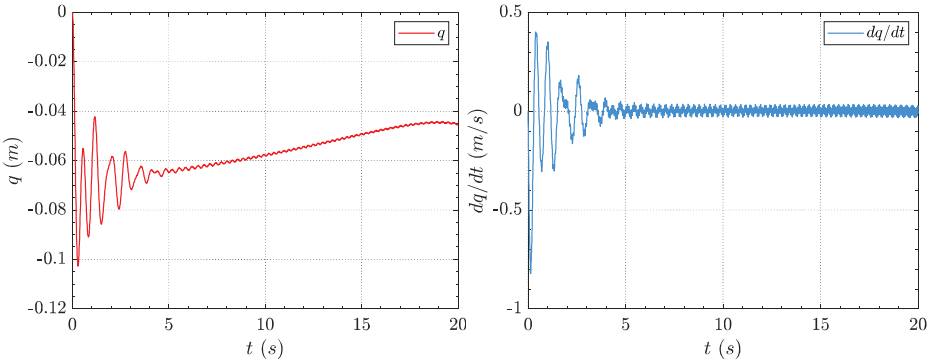

Fig. 3 Vertical displacement and velocity of the center of mass of m_1

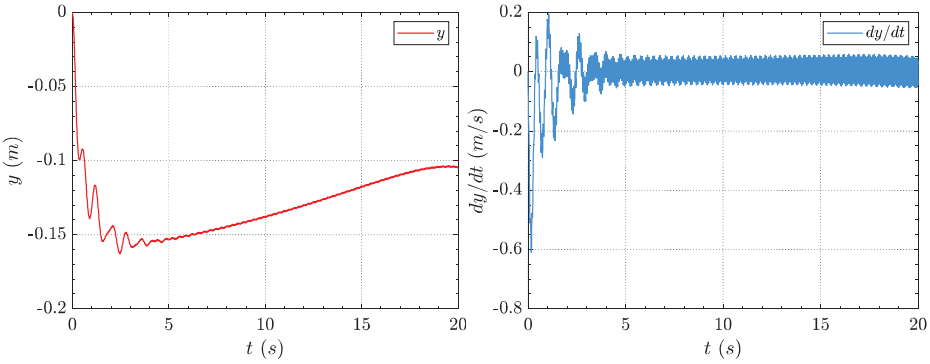

Fig. 4 Vertical displacement and velocity of the center of mass of m_2

In Fig. 3, the oscillation of the unsprung mass of the front axle gradually damps, with a stable oscillation amplitude in the seconds from 05 to 20, corresponding to very small oscillation velocities around 0.05 m/s. The final position of the center of mass of m_1 at the end of this phase is about 4.5 cm lower than the initial position.

In Fig. 4, we observe that the vertical displacement of the chassis reaches its maximum value of about 16 cm, with a stable oscillation amplitude in the seconds from 4 to 20, corresponding to very small oscillation velocities around 0.06 m/s. The pitch angle of the chassis reaches its maximum value of about 2.6° at the beginning of the lowering phase, and then stabilizes with a small amplitude (Fig. 5), with an angular

velocity during the stable phase around 0.08 rad/s. At the end of the lowering phase, the position of the center of mass of m_2 is about 10.5 cm lower than the initial position, and the chassis is tilted at an angle of about 1.66° relative to the horizontal.

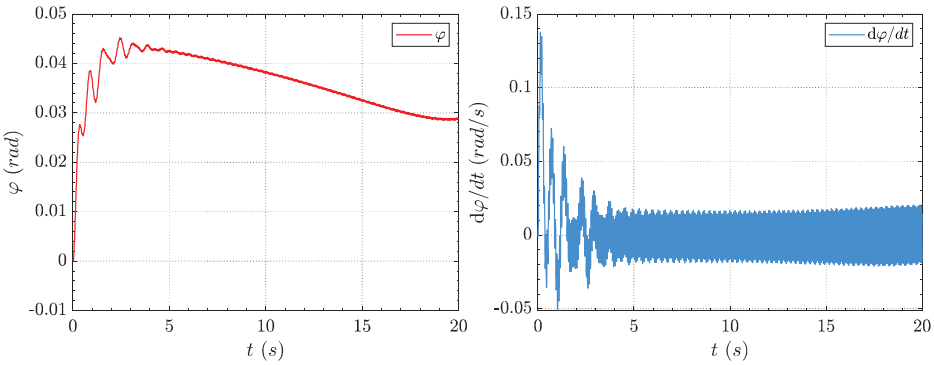

Fig. 5 Pitch angle and angular velocity of the chassis

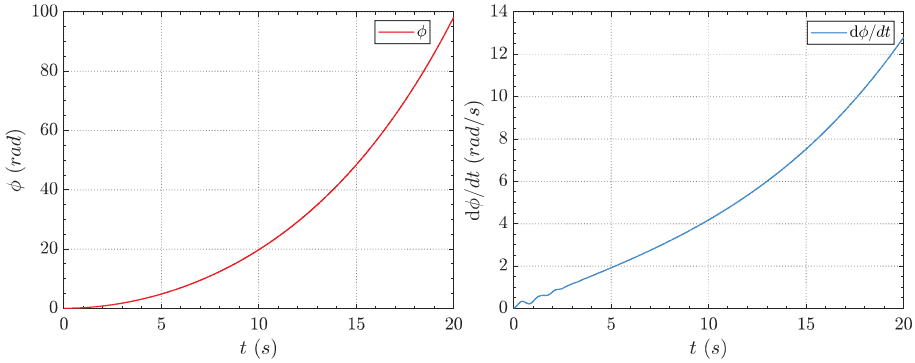

Fig. 6 Angular displacement and angular velocity of the drum

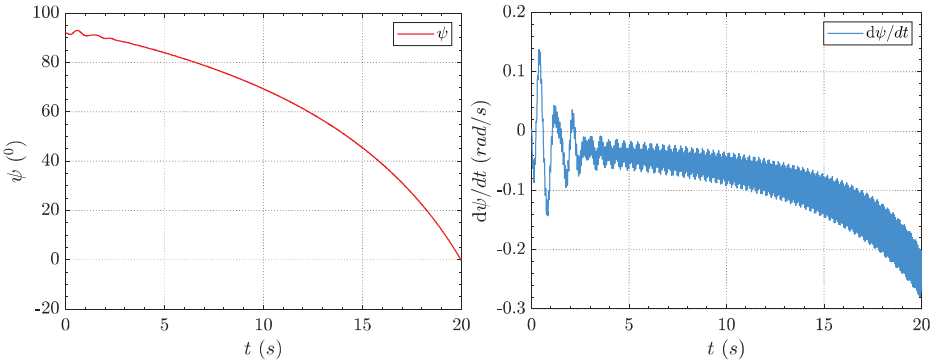

Fig. 7 Angular displacement and angular velocity of the bridge span

Throughout the entire span–lowering process, the rotation angle of the drum gradually increases from 0 to 98 rad, equivalent to 15.6 revolutions of the drum

(Fig. 6). The length of the cable wound onto the drum can be calculated to be approximately 9.8 m, which is a result consistent with practical operations.

During the span–lowering process, due to the elasticity of the cable, the rotation angle ψ determining the position of the bridge span undergoes oscillations, decreasing from the initial value of 92° to 0°. However, the oscillation amplitude is small (Fig. 7). At the beginning of the lowering phase, the amplitude of the rotation angle ψ undergoes changes corresponding to the oscillation of the chassis.

4 Conclusion

The paper has presented a dynamic model and established a system of differential equations describing the oscillations of a heavy mechanized bridge during the span-lowering process. With this model, it is possible to study the oscillations of the unsprung mass of the front axle, the chassis, and the bridge span. The obtained results of the paper can serve as a basis for improvement of the rear outriggers of the equipment and solution of both computational design problems, and the control problem of the cable winding drum to increase the lowering speed while ensuring the stability. These ideas will be further explored by the authors in future research.

References

[1] KALANGI, C. and Y. SIDAGAM. Design and Analysis of Armored Vehicle Launched Bridge (AVLB) for Static Loads. *International Journal for Scientific Research & Development*, 2016, **4**(10), pp. 9-18. ISSN 2321-0613.

[2] HAN, J., P. ZHU, L. TAO, G. CHEN, S. ZHANG and X. YANG. An Optimum Design Method for a New Deployable Mechanism in Scissors Bridge. *Proceedings of the Institution of Mechanical Engineers, Part C: Journal of Mechanical Engineering Science*, 2019, **233**(19-20), pp. 6953-6966. DOI 10.1177/0954406219869046.

[3] BAI, H.Y., C.Y. FU and X.Z. ZHANG. Kinematics Analysis of Heavy Dump Truck Lifting Mechanism. *Advanced Materials Research*, 2012, **472-475**, pp. 2245-2250, DOI 10.4028/www.scientific.net/AMR.472-475.2245.

[4] DUONG, L.V. and L.A. TUAN. Modeling and Observer–Based Robust Controllers for Telescopic Truck Cranes. *Mechanism and Machine Theory,* 2022, **173**, 104869. DOI 10.1016/j.mechmachtheory.2022.104869.

[5] SZELKA, J. and A. WYSOCZAŃSKI. Modern Structures of Military Logistic Bridges. *Open Engineering*, 2022, **12**(1), pp. 1106-1112. DOI 10.1515/eng-2022-0391.

[6] TUAN, L.A. and S.-G. LEE. Modeling and Advanced Sliding Mode Controls of Crawler Cranes Considering Wire Rope Elasticity and Complicated Operations. *Mechanical Systems and Signal Processing*, 2018, **103**, pp. 250-263, DOI 10.1016/j.ymssp.2017.09.045.

[7] TUAN, L.A. Fractional–Order Fast Terminal Back–Stepping Sliding Mode Control of Crawler Cranes. *Mechanism and Machine Theory*, 2019, **137**, pp. 297-314. DOI 10.1016/j.mechmachtheory.2019.03.027.

[8] TUAN, L.A., H.M. CUONG, S.-G. LEE, L.C. NHO and K. MOON. Nonlinear Feedback Control of Container Crane Mounted on Elastic Foundation with the Flexibility of Suspended Cable. *Journal of Vibration and Control*, 2014, **22**(13), pp. 3067-3078. DOI 10.1177/1077546314558499.

[9] XIN, Y. G. XU, N. SU and Q. DONG. Nonlinear Vibration of Ladle Crane Due to a Moving Trolley. *Mathematical Problems in Engineering*, 2018, **4**, 5756180. DOI 10.1155/2018/5756180.

[10] KIM, Y.J., R. TANOVIC and R.G. WIGHT. Load Configuration and Lateral Distribution of NATO Wheeled Military Trucks for Steel I-Girder Bridges. *Journal of Bridge Engineering*, 2010, **15**(6), pp. 740-748. DOI 10.1061/(ASCE)BE.1943-5592.0000113.

[11] NOR, N.M., A.A.M.A. ZAIDI, S. ABDULLAH, M.A. YUSOF and R.M. SOHAIMI. Static Analysis and Design of Sandwiched Composite Long–Span Portable Beam. *International Journal of the Physical Sciences*, 2011, **6**(27), pp. 6323-6328. DOI 10.5897/IJPS11.129.

[12] HOANG, Q.-D., S.H. WOO, S.-G. LEE, A.-T. LE, D.-T. PHAM, T.-V. MAI and V.-T. NGUYEN. Robust Control with a Novel 6-DOF Dynamic Model of Indoor Bridge Crane for Suppressing Vertical Vibration. *Journal of the Brazilian Society of Mechanical Sciences and Engineering*, 2022, **44**, 169. DOI 10.1007/s40430-022-03465-3.